## EDGE ARTICLE

Check for updates

# Deciphering the endogenous SUMO-1 landscape: a novel combinatorial peptide enrichment strategy for global profiling and disease association†

Xiaoyu Zhang, ‡[a] Bowen Zhong,‡[ae] Yue Sun,[a] Dan Liu,[a] Xiancheng Zhang,[a] Dongdong Wang,[a] Cunli Wang,[a] Huiling Gao,[c] Manli Zhong,[c] Haijuan Qin,[d] Yang Chen,[a] Zhiying Yang,[ab] Yan Li,[a] Haijie Wei,[ab] Xindi Yang,[a] Yukui Zhang,[a] Bo Jiang, *[a] Lihua Zhang *[a] and Guangyan Qing *[a]

Small ubiquitin-like modifier (SUMO) plays a pivotal role in diverse cellular processes and is implicated in diseases such as cancer and neurodegenerative disorders. However, large-scale identification of endogenous SUMO-1 faces challenges due to limited enrichment methods and its lower abundance compared to SUMO-2/3. Here we propose a novel combinatorial peptide strategy, combined with anti-adhesive polymer development, to enrich endogenous SUMO-1 modified peptides, revealing a comprehensive SUMOylation landscape. Utilizing phage display, we successfully identified a linear 12-mer and a cystine-linked cyclic 7-mer peptide ligand, specifically designed to target the C-terminal regions of SUMO-1 remnants. Building upon their high affinities and satisfactory complementarity, we developed the first artificial SUMO-1 enrichment materials, ultimately establishing a combinatorial peptide strategy that facilitates a comprehensive analysis of the endogenous SUMO-1 modified proteome in both cellular and tissue contexts. We successfully mapped 1312 SUMOylation sites in HeLa cells and 1365 along with 991 endogenous SUMOylation proteins in Alzheimer's disease (AD) mouse brain tissues. Notably, our method uncovered a significant upregulation of SUMO-1 in AD mouse brain tissue, providing new insights into SUMOylation's role in disease. Overall, this work represents the most thorough exploration of SUMO-1 modified proteomics and offers robust tools for elucidating the roles of SUMO-1's biological significance.

## Introduction

Protein SUMOylation, also known as small ubiquitin-like modifier (SUMO, ~12 kD) modification, is a critical post-translational modification (PTM) present in all eukaryotes. Several important proteins, such as the well-known p53, Ran-GAP1, and PIAS1, have been reported or speculated to undergo SUMOylation.[1,2] The widespread occurrence of SUMOylation

*[a]State Key Laboratory of Medical Proteomics, National Chromatographic R. & A. Center, CAS Key Laboratory of Separation Science for Analytical Chemistry, Dalian Institute of Chemical Physics, Chinese Academy of Sciences, Dalian 116023, P. R. China. E-mail: jiangbo@dicp.ac.cn; lihuazhang@dicp.ac.cn; qinggy@dicp.ac.cn*

*[b]University of Chinese Academy of Sciences, Beijing 100039, P. R. China*

*[c]College of Life and Health Sciences, Northeastern University, Shenyang 110819, P. R. China*

*[d]Research Centre of Modern Analytical Technology, Tianjin University of Science and Technology, Tianjin 300000, P. R. China*

*[e]School of Chemistry and Materials Science, University of Science and Technology of China, Hefei 230026, P. R. China*

† Electronic supplementary information (ESI) available. See DOI: https://doi.org/10.1039/d4sc07379g

‡ X. Z. and B. Z. contributed equally to this work.

highlights its crucial role in regulating various cellular processes, including DNA repair, gene expression, protein stability and trafficking, signal transduction, and stress responses.[3,4] Dysregulation of SUMOylation has been implicated in a range of diseases, including cancers, metabolic disorders, and neurodegenerative conditions.[5] Notably, the first drug that blocks SUMOylation is currently under investigation in clinical trials as a potential anti-cancer agent.[6] Given the crucial role of SUMOylation in diverse biological processes and its implication in diseases, it is imperative to gain a comprehensive understanding of the mechanisms underlying SUMOylation, elucidating the specific sites of SUMO modification, and uncovering the precise roles of SUMOylation in various biological processes, which could open new avenues for targeting SUMO in disease treatment.

SUMO proteins are highly conserved across eukaryotic organisms. In mammalian cells, three major SUMO paralogs are expressed: SUMO-1, SUMO-2, and SUMO-3. SUMO-2 and SUMO-3 share 95% sequence identity, while SUMO-1 has only 45% sequence homology with SUMO-2/3. Although they all use a similar conjugation mechanism, their substrate specificities and functional impacts contribute differently to cellular

processes and responses.[7,8] Research has confirmed that SUMO-1 modification primarily occurs through substrate conjugation, and it predominantly exists in a covalently modified state rather than in a free form.[7,9] However, due to current research limitations in enriching SUMO-1 from complex samples and its lower abundance, the numbers of SUMO-1 modification sites and substrate proteins are only about 1% of those found for SUMO-2/3. The majority of current SUMO-related information overwhelmingly focuses on SUMO-2/3. SUMO-1 is considered a great treasure trove, yet our understanding of it remains very limited thus far. Therefore, the establishment of methods for identifying SUMO-1 modifications presents a significant challenge but is of utmost importance for advancing our knowledge of SUMO-mediated cellular processes and their potential roles in disease.

Major PTMs such as phosphorylation,[10–12] ubiquitylation,[13,14] glycosylation,[15–17] and acetylation[18] have well-established enrichment and identification methods, revealing tens of thousands of endogenous modification sites, which have significantly advanced biomarker discovery and drug development.[19,20] However, the site-specific identification of SUMOylation, particularly SUMO-1, remains significantly limited, with only a few dozen to a few hundred endogenous modification sites identified. The most successful enrichment and analysis approaches in SUMOylation proteomics to date have been through the introduction of enrichment tags on SUMO and mutating specific amino acids.[21–23] However, introducing exogenous SUMO into an organism cannot accurately reflect the real expression level and dynamic changes of SUMO modification in the organism, nor can it be used for the analysis of clinical and tissue samples.[9]

Consequently, significant attention has been given to studying the enrichment strategies for SUMO-modified peptides at the endogenous level. Notable studies by Cai et al.,[8] Lumpkin et al.[24] and Hendriks et al.[25] represent some of the few that focus on identifying endogenous SUMO modifications. Cai et al. developed an anti-pan-SUMO-1 antibody to enrich SUMO-1 modifications, but its limited specificity resulted in minimal identification of endogenous SUMO-1 sites.[8] Lumpkin et al. identified numerous endogenous SUMO sites using a WaLP enzyme and anti-ubiquitination antibodies, though this method could not distinguish between different types of SUMOylation and risked false positives.[24] Hendriks et al. reported the largest number of endogenous SUMO-2/3 sites to date but provided no information on SUMO-1.[25] These efforts highlight the significant challenge and importance of accurately identifying endogenous SUMO-1 modifications, which remain underrepresented due to technical limitations and the lower abundance of SUMO-1 compared to SUMO-2/3. It is worth noting that the enrichment strategies in these current studies all rely on antibodies. Antibodies, however, possess inherent limitations such as restricted specificity, limited availability, biological variability, and technical constraints.[26] Currently, there are no efficient artificial materials available for the selective enrichment of SUMO-1 modified peptides, further compounding the difficulties in comprehensively identifying endogenous SUMO-1 modification sites from complex biological samples.

Here, we address these gaps by pioneering a novel combinatorial peptide strategy for enriching and identifying endogenous SUMO-1 modifications applicable to both cellular and tissue contexts. Leveraging phage display screening and functional material design, we developed specific peptide ligands targeting the C-terminal regions of SUMO-1 remnants (Fig. 1a and b). For the linear 12-mer sequence, we utilized a 12-mer peptide library, while a shorter, more rigid cyclic heptapeptide library was employed for the QTGG. This divide-and-conquer approach not only ensures high specificity in SUMO-1 peptide enrichment but also facilitates subsequent mass spectrometry (MS) identification. The combinatorial strategy is grounded in meticulous material design, enabling robust capture of endogenous SUMO-1 modified peptides for comprehensive proteomic analysis (Fig. 1c). Ultimately, this high-throughput, peptide-based method allowed for an unprecedented investigation of SUMO-1 modifications applied to HeLa cells as well as brain tissues from Alzheimer's disease (AD) mouse models (expressing the human MAPTP301S transgene). Our results reveal a comprehensive SUMO-1 modified proteome in both cellular and disease-relevant contexts, marking the most extensive exploration of endogenous SUMO-1 proteomics to date.

## Results and discussion

### Target design for phage display

For ubiquitination, commercial K-GG antibodies can be used to enrich diglycine modified peptides.[27] However, for SUMO-1 modified peptide purification, antibodies are not commercially available. Peptide ligands provide an alternative class of molecules that can bind to specific targets with high affinity, similar to antibodies. Phage display technology, renowned for its ability to identify such ligands with high specificity and affinity, is a powerful screening method.[28,29] In this study, to select binding peptides targeting SUMO-1 modified peptides, the C-terminus of SUMO-1 remnants "DVIEVYQEQTGG" and "QTGG" (the last glycine is respectively covalently conjugated to the lysine residues of substrate proteins) were used as antigens for selection from the phage display peptide library, respectively (Fig. 1a).

### Identification of peptide ligands which bind to DV12

For relatively long remnant DVIEVYQEQTGG (named as DV12), MS and high-performance liquid chromatography (HPLC) data for DV12 are shown in Fig. S1 in the ESI;† the dodecapeptide (Ph.D.-12) library was used to screen against DV12 through a complete biopanning procedure (Fig. 1b). The library has complexities on the order of $\sim10^9$ independent clones, which is sufficient to encode most if not all of the possible 12-mer peptide sequences (contained $\sim2 \times 10^{11}$ unique linear 12-mer peptides).[30] In the biopanning procedure, bovine serum albumin (BSA) was used to eliminate non-specific phages. Then four rounds of affinity selection against DV12 were carried out. By measuring the phage recovery ratio after each round of
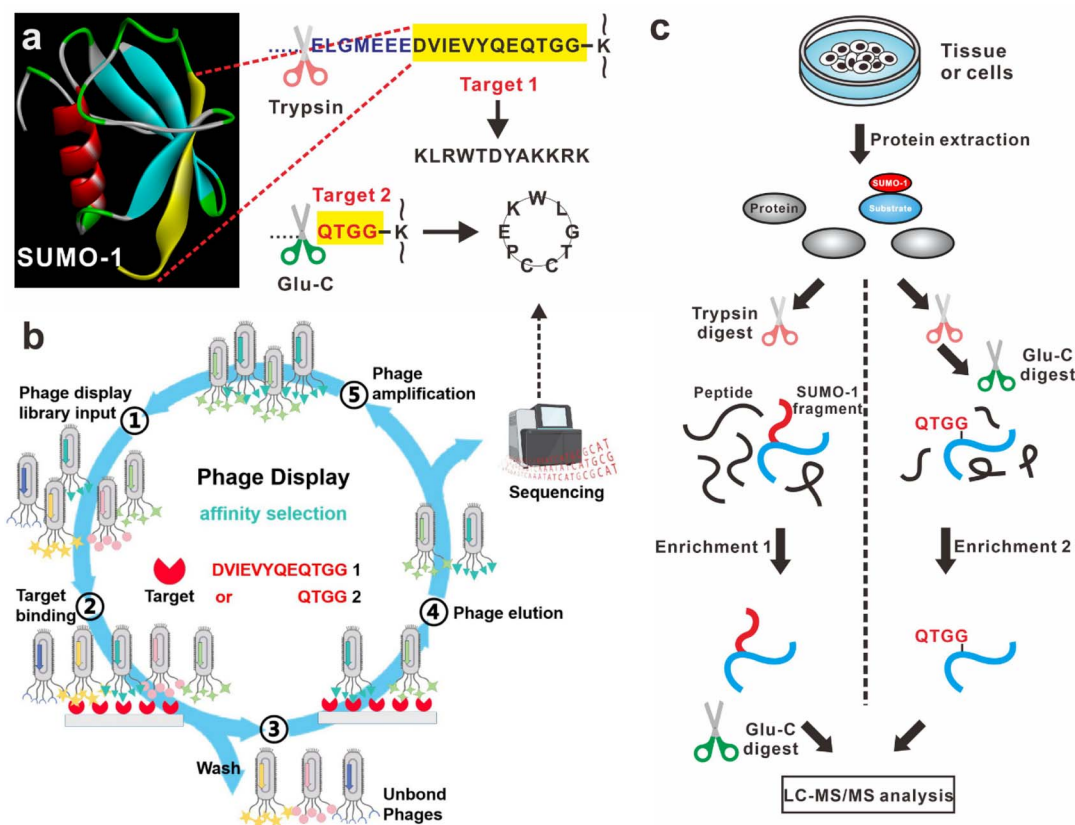
Fig. 1 Scheme of material design for deciphering the endogenous SUMO-1 landscape. (a) The C-terminus of SUMO-1 remnants "DVIEVY-QEQTGG" and "QTGG" were selected as targets, respectively. (b) Biopanning for peptide ligands against the selected targets through phage display technology. (c) Development of a peptide-based strategy for enriching endogenous SUMO-1 modified peptides.

biopanning, the enrichment of the phages toward DV12 could be assessed. The iterative affinity biopanning cycle resulted in a gradually increased phage recovery ratio. After four rounds, the increased phage recovery ratio indicated the successful selection (Table S1 in the ESI†). After that, 16 phage clones were randomly selected for sequencing from round 4. Fig. 2a lists amino acid sequences of the identified peptides, and their relative occurrence frequencies. Sequences of clones 1# and 2# were repeated four and three times, respectively. The obtained chemical diversity offers a comprehensive under-standing of the general characteristics of the binders.[31] The sequences presented here are reported for the first time, no known motif was identified upon alignment with the protein Basic Local Alignment Search Tool (BLAST) database search.

The binding affinity of the above phage monoclones which bear identified peptides toward DV12 was preliminarily evaluated by the phage enzyme-linked immunosorbent assay (ELISA). Among the tested binders, 2#, 4#, 8#, and 10# exhibited the highest affinity toward DV12 (Fig. 2b). The above corresponding four candidate peptides (namely PEP-1–PEP-4) were subsequently synthesized by solid-phase peptide synthesis. Besides, the peptide sequence corresponding to the weakest binding phage (7#) was also synthesized as a negative control (PEP-5). The synthesized peptides were characterized through HPLC and MS (Fig. S2 in the ESI†). In the following studies, we aimed

to quantify binding and understand the interaction with the target DV12.

First, the biolayer interferometry (BLI) assay[32,33] was used to investigate the binding affinities between these peptides and DV12. Dynamic response curves display rapid and intensive adsorption of peptides on the DV12-modified sensor surfaces, corresponding to their high association rate constants ($K_{on}$), meanwhile low dissociation rate constants ($K_{off}$) (Fig. 2c) were observed when these peptides were eluted from the sensor surfaces (Fig. 2d and S3 in the ESI†). A lower $K_D$ ($K_{on}/K_{off}$) indicated a stronger binding affinity. Peptides bound to DV12 with high affinities (PEP-1, $K_D$: 124 nM; PEP-2, $K_D$: 837 nM; PEP-3, $K_D$: 88.5 nM; PEP-4, $K_D$: 2.0 nM) revealed the strong binding, which was comparable to that of antibodies. Notably, PEP-4 (KLRWTDYAKKRK) exhibited the strongest binding affinity to DV12, while no measurable affinity was obtained for PEP-5 (negative control peptide) (Fig. 2e). Therefore, the mode of interaction of PEP-4 with DV12 was then studied in more detail.

Initially, we investigated the possible binding sites between PEP-4 and DV12 using hydrogen nuclear magnetic resonance ($^1$H NMR) titration. We assigned the chemical shift attribution of each H proton in PEP-4 and DV12 based on $^1$H–$^1$H total correlation NMR spectra and $^{13}$C–$^1$H heteronuclear singular quantum correlation (HSQC) NMR spectra (Fig. S4 in the ESI†). Then, the chemical shift variations of these H protons were
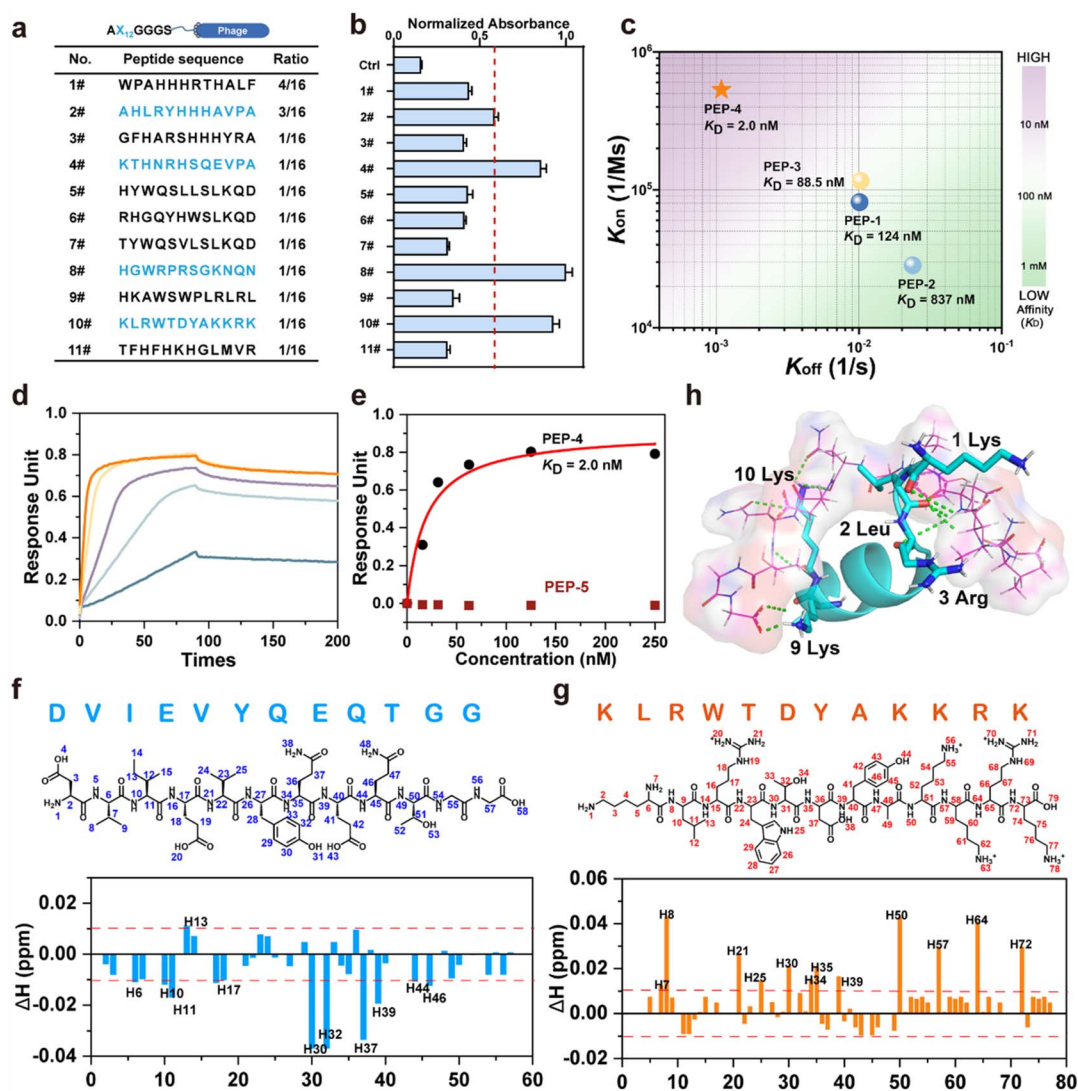
Fig. 2 Selection and characterization of the DV12-binding peptide. (a) Sequences and frequencies of the peptides obtained from phage display selection against DV12. (b) Binding affinities of the selected binding phages to DV12 via ELISA. Binding affinity was represented by the normalized absorbance at 405 nm. The data are presented as mean ± SD of 3 independent experiments. (c) Heatmap of the binding affinities of the selected peptides: the association rate constant ($K_{on}$) is plotted against the dissociation rate constant ($K_{off}$), and the color bar corresponds to the value of the equilibrium constant ($K_D$, calculated as $K_{off}/K_{on}$ using 1 : 1 binding model). (d) PEP-4 association and dissociation kinetics at different concentrations (15.6, 31.3, 62.5, 125, and 250 μM) on DV12-modified sensor surfaces, recorded by BLI tests. (e) BLI fitting curves of PEP-4 (black) or PEP-5 (red) interacted with DV12. (f and g) $^1$H NMR chemical shift variations in DV12 (f) and PEP-4 (g) upon complexation. The peptide concentrations were 20 mM in dimethyl sulfoxide-$d_6$, temperature: 25 °C. (h) Possible binding model between PEP-4 (shown as pink lines and surface) and DV12 (shown as blue sticks) demonstrated by PyMOL, obtained through molecular docking using AutoDock. Hydrogen bonds are displayed as green dashed lines with different lengths (Table S2 in the ESI†).

recorded after interaction with an equimolar amount of DV12 as shown in Fig. 2f and g. Significant alterations in the chemical shifts belonged to residues isoleucine (3I), glutamic acid (4E, 8E), tyrosine (6Y) and glutamine (7Q, 9Q) in DV12, and residues leucine (2L), arginine (3R, 11R), threonine (5T) and lysine (9K, 10K, 12K) in PEP-4, indicating a strong intermolecular interaction. Subsequently, guided by this information, we performed molecular docking (MD) simulations to gain a possible binding model between PEP-4 and DV12 (Fig. 2h). Our analysis revealed that the residues 3 (isoleucine), 4 (glutamic acid), 7, 9 (glutamine), 10 (threonine), and 12 (glycine) in DV12 interacted with

the residues 1 (lysine), 2 (leucine), 3 (arginine), and 9, 10 (lysine) in PEP-4, forming a total of 11 sets of hydrogen bonds between them, being consistent with the NMR findings.

## Identification of peptide ligands which bind to QTGG

In the bottom-up protein profiling strategy, the SUMO-modified amino acid sequence remains very long (SUMO-1 and SUMO-2/3 modifications retain 19 and 32 amino acids respectively) on the substrate peptide after SUMO proteins are cleaved by trypsin, which makes it difficult to be detected and analyzed by MS, thus seriously affecting the analysis coverage of SUMO proteins in

mammals.[34] Usually, to reduce the length of SUMO-1 modified peptides, a second protease digestion step was performed by Glu-C to further trim the SUMO-1 peptide side chain to QTGG, thereby making it more compatible with MS identification.[4] Importantly, this step helps to filter out SUMO-2/3 modified peptides, as Glu-C cannot cleave at their C-termini to generate the QTGG short peptide. Consequently, we subsequently selected QTGG as the target for phage display screening to obtain peptides that specifically bind to this modified segment, thus facilitating peptide enrichment and MS identification.

For this relatively short remnant, the smaller the molecule, the more challenging it becomes to obtain its ligand through phage display. The specificity and binding strength of such ligands depend heavily on the diversity and design of the peptide library. For extremely small targets, incorporating structural constraints into the library, such as cyclic or stapled peptides, is crucial. Accordingly, we opted for a shorter and more rigid loop-constrained heptapeptide (Ph.D.-C7C) library to screen against QTGG, following a complete biopanning procedure similar to the one used for DV12 (Fig. 1b). The Ph.D.-C7C library's randomized segment is flanked by a pair of cysteine residues. During phage assembly, these cysteine residues undergo oxidation, forming a disulfide linkage that presents the displayed peptides to the target in loop configurations. After three rounds of biopanning, ten phage clones were randomly selected for sequencing and analyzed, leading to 7 newly displayed peptide sequences (Fig. 3a). Through phage ELISA (Fig. 3b) and isothermal calorimetry (ITC) (Fig. 3c–f and S5 in the ESI†), CPEKWLGTC (named CP-1) exhibited a stronger binding affinity ($K_D$: 71.78 nM) compared to CMTPNPTTC (named CP-2, $K_D$: 1.8 μM) and LP-1 ($K_D$: 122.8 nM) which corresponds to the linear form of CP-1, underscoring the essential role of the rigid cyclic structure in molecular recognition. It is worth noting that here we adopted ITC to measure the $K_D$ values because ITC is more suitable for interactions involving small molecules. By comparison, BLI is more appropriate for studying macromolecular interactions and could not provide reliable data for the complexation between QTGG and the cyclic peptides due to minor variations in the responding signal. Subsequently, the possible interaction model between CP-1 and QTGG was investigated by 2D $^1$H–$^1$H total correlation NMR spectroscopy (Fig. 3g, h and S6 in the ESI†) and MD simulations (Fig. 3i), confirming the robust binding between CP-1 and QTGG. The detailed description is illustrated in ESI Note 1 in the ESI.† Taken together, through phage display, we have successfully identified a group of peptide ligands that specifically recognize oligopeptides left on the SUMO-1 modified substrate peptide.

## Materials design

Generally, the abundance of SUMOylated peptides in practical bio-samples is quite low, often at the nanomole level, and their enrichment will encounter serious interference from other proteins or peptides. To tackle this challenge, we proposed a design of functional polymer to incorporate our peptide ligands. Here poly(ethylene glycol) methyl ether acrylate

(PEGMEA) was chosen as the polymer main chain because of its excellent resistance to protein adsorption, further PEGMEA was allowed to copolymerize with glycidyl methacrylate (GMA), and the screened peptide ligands could be grafted onto the copolymer through a ring-opening reaction with the epoxy groups of GMA.[35,36] This design significantly increased the number of available peptide ligands for interactions with the targets and endowed the excellent antifouling ability to the enrichment material. As depicted in Fig. 3j, SiO$_2$@poly(PEGMEA-co-GMA) was prepared via surface reversible addition-fragmentation chain transfer (RAFT) polymerization on a porous silica microsphere substrate. Subsequently, Pep-4 or CP-1 was grafted to the copolymers, resulting in two kinds of enrichment materials based on silica gels. For clarity in subsequent discussions, we denote the material modified with PEP-4 as **M1** and that modified with CP-1 as **M2**, respectively. The detailed characterization data, along with the binding affinity and specificity of the materials, are provided in Fig. S7 and S8,† as well as ESI Note 2 in the ESI.†

## Establishment of the combinatorial peptide enrichment strategy

Initially, targeting model peptides, enrichment methods were established based on **M1** and **M2**, and the detailed description could be found in Fig. S9 and S10, ESI Note 3 in the ESI.† Then we conducted comprehensive profiling of endogenous SUMO-1 modifications under standard cell culture conditions (control) and the treatment of the proteasomal inhibitor MG132 capable of increasing SUMO-1 expression levels (MG132) respectively. The peptide mixtures were enriched by **M1** or **M2**, and the detailed workflow is shown in Fig. S11 in the ESI.† In our experimental, **M1** was used to capture SUMO-1 modified peptides, in combination with the enhanced Glu-C digestion to cut the tryptic SUMO-1 remnant into the QTGG-remnant, which is more conducive to MS identification. In a parallel experiment, **M2** was utilized to capture the QTGG- remnant after trypsin and Glu-C digestion. From the **M1**-dependent workflow, we identified 54 and 223 SUMO-1 modified sites (Fig. 4a and ESI Data set 1†) in the control and MG132 stimulation groups, respectively. Correspondingly, we identified 209 and 351 SUMO1-modified sites using the **M2**-dependent workflow (Fig. 4b and ESI Data set 1†). Subsequently, we compared the SUMO-1 modified sites identified by the **M1**- and **M2**-dependent workflows. As illustrated in Fig. 4c, the overlap between **M1**- and **M2**-dependent workflows was relatively low in both the control and MG132 stimulation groups, which is favorable for the subsequent establishment of the combinatorial peptide enrichment strategy. The detailed description on the overlap is shown in Fig. S12 and ESI Note 4.†

Consequently, we merged the SUMO-1 modified proteins identified by both materials for Gene Ontology (GO) analysis (ESI Data set 2†). According to the enrichment analysis of cellular components by metascape,[37] proteins located in the centrosome, axon, myofibril, proteasome complex, and microtube showed a significant increase in SUMO-1 modification (Fig. S13a in the ESI†). With regard to the biological process
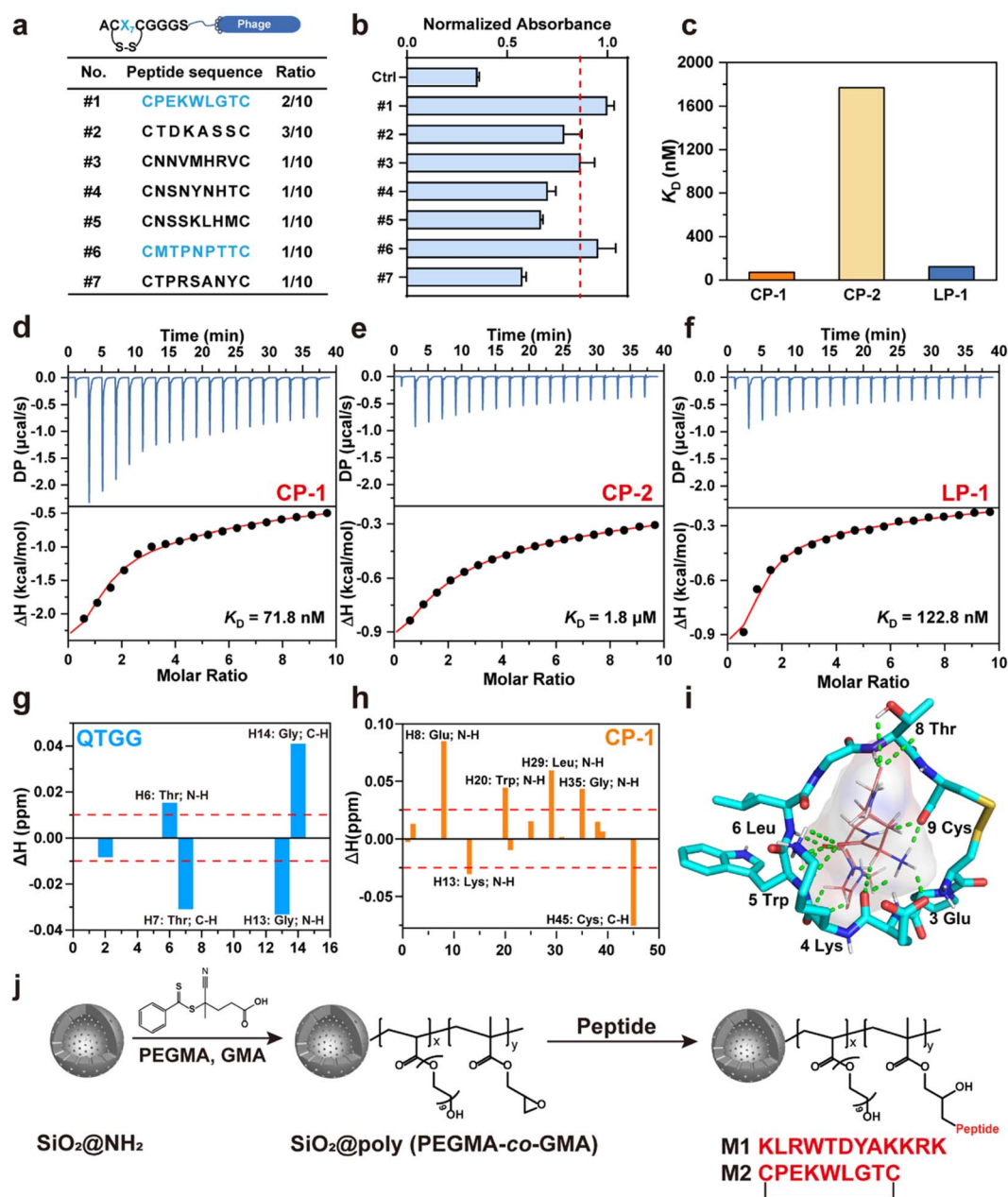
**Fig. 3** Selection and characterization of the QTGG-binding peptide. (a) Sequences and frequencies of the peptides obtained from phage display selection against QTGG. (b) Binding affinities of the selected binding phages to QTGG *via* ELISA, represented by the normalized absorbance at 405 nm. The data are presented as mean ± SD of 3 independent experiments. (c) Comparison of the equilibrium constant ($K_D$) of the selected peptides obtained by ITC. (d–f) ITC raw data and the corresponding fitting curves of QTGG upon the titration of CP-1 (CPEKWLGTC) (d), CP-2 (CMTPNPTTC) (e), and LP-1 (linear form of CP-1) (f), respectively, in $H_2O$ at 25 °C. (g and h) ^{1}H NMR chemical shift variations in QTGG (g) and CP-1 (h) upon complexation. The peptide concentrations were 20 mM in dimethyl sulfoxide-$d_6$, temperature: 25 °C. (i) Possible binding model between CP-1 (shown as blue sticks) and QTGG (shown as pink lines and surface) demonstrated by PyMOL, obtained through molecular docking using AutoDock. Binding interactions are displayed as green dashed lines with different lengths (Table S4 in the ESI†). (j) Schematic illustration of the synthesis process for the functional polymer incorporating PEP-4 (**M1**) and CP-1 (**M2**) on silica microsphere substrates (Fuji Silysia Chemical, Japan, $NH_2$ SPS300-5; average particle size: 5 μm; inner pore diameter: 300 Å; surface area: 90 $m^2$ $g^{-1}$; pore volume: 0.80 mL $g^{-1}$).

(Fig. S13b in the ESI†), more proteins were involved in the process of chromosome segregation, microtubule cytoskeleton organization, protein phosphorylation, cellular component morphogenesis, and the ubiquitin-dependent protein catabolic process in response to MG132 stimulation. In terms of molecular function (Fig. S13c in the ESI†), proteins with the functions

of protein kinase activity, GTPase regulator activity, and microtubule binding were more likely to be modified by the SUMO-1 protein. Therefore, significant biological changes occurred after MG132 stimulation, leading to increased levels of SUMO-1 modification, suggesting enhanced regulation by SUMO-1 in biological systems. This regulation mainly focuses
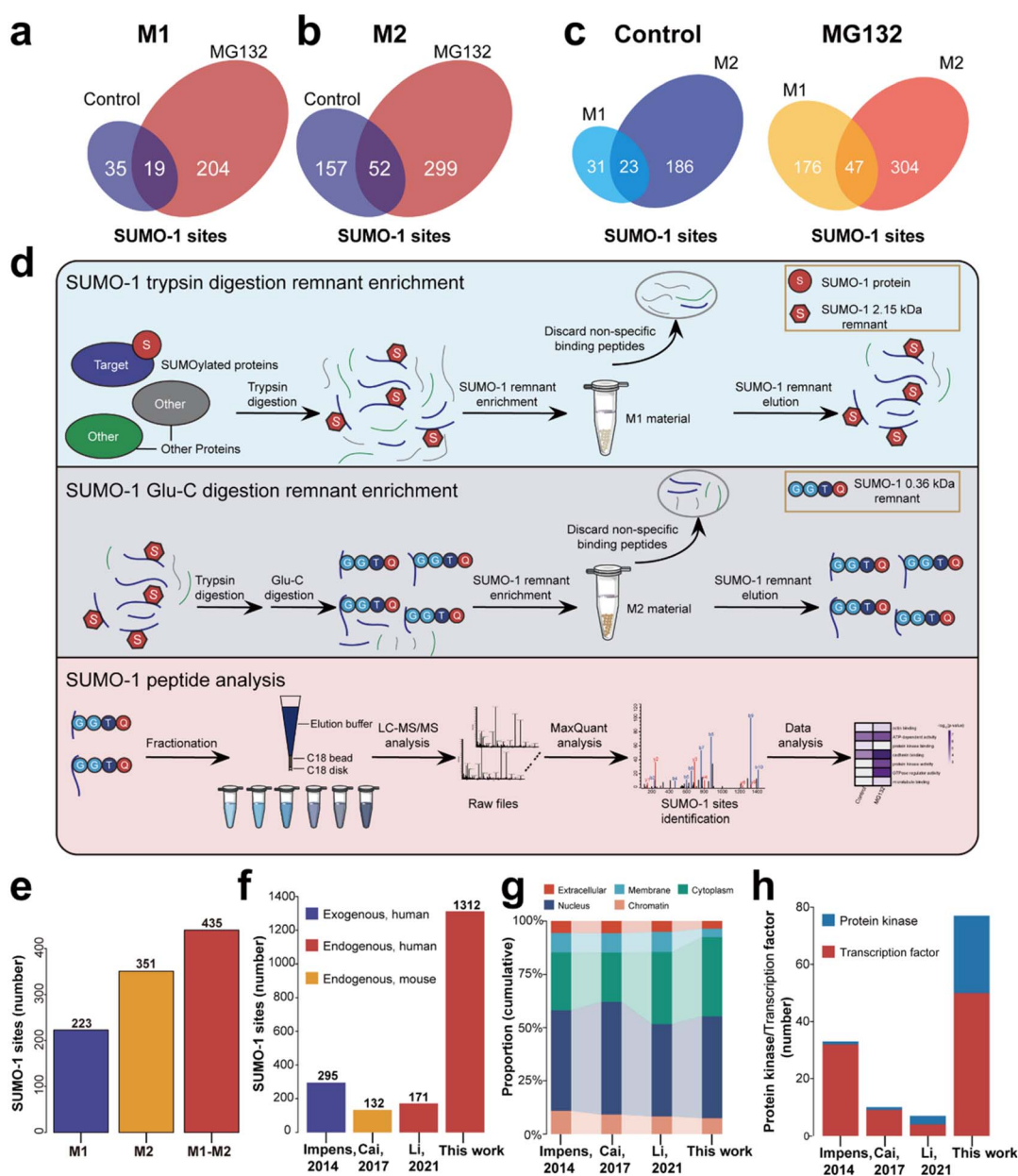
Fig. 4 Combinatorial peptide strategy for the enrichment of endogenous SUMO-1 modified sites. (a and b) SUMO-1 modified sites identified with **M1**-dependent (a) and **M2**-dependent methods (b) from digested proteins extracted from HeLa cells before (blue circles) and after MG132 stimulation (purple circles). (c) Overlap of SUMO-1 modified sites between **M1** and **M2** in control and MG132 stimulation groups. (d) Schematic overview of the combinatorial peptide enrichment strategy. (e) Comparison of the number of SUMO-1 modified sites identified by **M1**-dependent, **M2**-dependent, and two-step sequential enrichment methods in HeLa cells under MG132 stimulation. (f) Comparison of the number of SUMO-1 modified sites identified in our work with other relevant studies. (g) Subcellular localization analysis was conducted using Gene Ontology Cellular Component (GOCC). SUMO-1 modified proteins were categorized into various localizations based on GOCC terms, ranging from chroma-tin-associated with extracellular components. (h) Comparison of the number of protein kinase and transcription factors among identified SUMO-1 modified proteins in our work with other relevant studies.

on the microtubule cytoskeleton, chromosome and DNA recombination, and protein kinase regulation, all of which are associated with various diseases. For instance, alterations in microtubule function are linked to many neurodegenerative diseases, while kinases are closely associated with various cancers. Taken together, our method was reliable, and it verified the widespread endogenous SUMO-1 modifications.

Considering the enrichment ability of **M1** and **M2** for different SUMO-1 remnants, respectively, we combined the properties of these two materials to establish a combinatorial peptide strategy, which may increase identification coverage. Thus, we comprehensively considered factors such as the pre-processing time increased by secondary enzymatic digestion, sample complexity, and MS signal quality, ultimately

establishing the combinatorial peptide strategy as illustrated in Fig. 4d. In this method, the **M1** material was used to retain SUMO-1 remnants after trypsin digestion, the collected elution was digested by Glu-C and then enriched by the **M2** material. This two-step sequential enrichment based on combinatorial peptides was able to increase the proportion of SUMO-1 modified peptides in the peptide mixture used for MS detection, which was better for enhancing the identification of low abundant SUMO-1 modified sites.

For a proof-of-concept demonstration, we applied this method to HeLa cells under MG132 stimulation. As we expected, the number of SUMO-1 modified sites was increased to 435, showing a significant increase compared to the methods using two materials alone (Fig. 4e and ESI Data set 1†). Notably, we conducted searches for SUMO-2/3 modifications and identified only 56 SUMO-2/3 sites among the 435 SUMO-1 modified sites. Given that SUMO-2/3 levels are significantly higher than those of SUMO-1, this distinction underscores the specificity of our method. Furthermore, we analyzed the adherence of identified SUMO-1 modified sites in the above three methods to the KxD/E consensus motif, as this commonly is considered an important benchmark in SUMO proteomics data.[38] We found that 10.1% to 14.3% (32, 41, 44) of the SUMO-1 modified sites were observed to occur on the consensus KxD/E motif, while 10.8% to 14.8% (33, 44, 47) of the SUMO-1 modified sites were observed to occur on the inverted consensus D/ExK motif (Fig. S14 in the ESI†). The adherence of the identified SUMO-1 modified sites to the consensus motif is consistent with previous identification results.[21] Additionally, we conducted a statistical comparison between our experimental results and the expected percentages in the human proteome. As summarized in Tables S6† and S7,† the percentages of both the consensus motif and the inverted consensus motif in the identified SUMO-1 modified sites are statistically significantly higher compared to the human proteome (ESI Note 5†). This analysis demonstrates that the enrichment of these motifs in our identified SUMO-1 modified sites is not random and further supports their relevance in SUMO-1 modification. Collectively, we confirmed both the necessity and the advancement of developing two types of enrichment materials, highlighting the reliability of our method. The combinatorial peptide strategy offers the potential for deep coverage of endogenous SUMO-1 proteome analysis.

## Comprehensive landscape of endogenous SUMO-1 modifications in HeLa cells

Overall, in our all HeLa cells dataset, we successfully identified a total of 1312 SUMO-1 sites and 1023 modified proteins in all **M1**-dependent, **M2**-dependent and three biological replicated two-step sequential enriching experiments. Compared to other endogenous SUMO-1 enrichment methods,[8,34] the number of identified SUMO-1 sites increased by at least 7 times (Fig. 4f and ESI Data set 3†). Additionally, when compared to exogenous SUMO-1 enrichment methods reported by Impens,[39] the identification counts also rose by 4.4 times. We conducted a comprehensive comparison of enrichment methods,

experimental conditions, initial protein amounts, and identification results across previous SUMO-1 enrichment studies (Table S8 in the ESI†). Notably, the HPLC and MS conditions used in our study are comparable to those reported in earlier studies. Furthermore, all studies, including ours, utilized the same MaxQuant software for database searching, applying consistent cutoff values for modification site identification. The significant increase in the number of endogenous SUMO-1 modification sites identified in our study is attributed to the combinatorial peptide enrichment method based on **M1** and **M2** materials that we developed. While significant differences might exist among SUMOylates obtained from various studies, we sought to elucidate whether there were commonalities among them. We compared the subcellular localization of SUMO-1 target proteins across different datasets (ESI Data set 3†). Overall, we observed globally consistent properties of SUMOylation, with a predominant nuclear localization (Fig. 4g). Those proteins were mainly located in the centrosome and microtubule, involved in the mitotic cell cycle, DNA damage response, and microtubule cytoskeleton organization, with the functions of ATP-dependent activity, GTPase regulator activity, and protein kinase binding (Fig. S15a in the ESI†). Furthermore, among the identified modified proteins, we observed a significant presence of protein kinases and transcription factors compared to other datasets (Fig. 4h and ESI Data set 3†).

The notable increase in modified protein kinases within our dataset remarkably enhances the depth and significance of our study. According to the BioGRID database, vital protein kinases and their interacting proteins were identified with SUMO-1 modification. Those proteins actively participate in crucial biological processes, including the mitotic cell cycle, regulation of DNA metabolic processes, mRNA metabolism, and protein phosphorylation (Fig. S16 in the ESI†). Notably, we identified that mitogen-activated protein kinase kinase 4 (MAP2K4) is subjected to SUMO-1 modification at the K118 site. As a member of the MAPKK family, MAP2K4 is involved in regulating the MAPK signaling pathway, whose dysregulated activity is closely associated with the initiation and progression of various cancers.[40] MAP2K4, in particular, is considered a promising drug target, and current research has been exploring the development of anti-cancer drugs targeting MAP2K4 to effectively treat tumors.[41] However, there is no research on the SUMO-1 modification of MAP2K4. Our findings provide new insights into MAP2K4 as a potential target for cancer therapy. The SUMO-1 modification of MAP2K4 may influence the biological behavior of cancer cells such as protein stability and biological function, consequently resulting in alterations in the regulation of corresponding signaling pathways. Therefore, investigating SUMO-1 modifications of protein kinases and their roles in cancer is crucial for gaining a deeper understanding of cancer etiology and identifying novel therapeutic targets.

Additionally, our study uncovered SUMO-1 protein modifications on several transcription factors. Transcription factors play a crucial role in gene expression regulation. They are proteins that bind to specific DNA sequences in the promoter or enhancer regions of genes and can either activate or repress the

transcription of those genes. This process is a key step in controlling when and to what extent genes are expressed.[42] In our dataset (Fig. S15b in the ESI and ESI Data set 3†), many transcription factors regulating the cell cycle and DNA damage response were found modified by the SUMO-1 protein, which also provided evidence for the regulation of SUMO-1 in the above biological processes.

### Discovery of endogenously SUMO-1 modified sites in Alzheimer's disease mouse brain tissue

Based on the data obtained from HeLa cells, a substantial portion of proteins modified by SUMO-1 is localized within the microtubule structure, where they intricately regulate the organization of the microtubule cytoskeleton. It is noteworthy that proteins associated with microtubules have established implications in the progression of Alzheimer's Disease (AD).[43,44] The treatment of AD remains a significant challenge, urgently necessitating the discovery of new potential targets and innovative therapeutic approaches. Therefore, studying the dynamic changes of SUMO-1 would help reveal the molecular mechanism of AD pathogenesis.[45,46] Here, we employed our combinatorial peptide strategy, achieving the first comprehensive proteomic identification of SUMO-1 modifications in an AD mice model to date.

We meticulously prepared two groups of 9 month-old mice C57BL/6 wild type (WT) and Tau P301S, corresponding to the healthy and AD model mice, to investigate SUMO-1 sites in mouse brain tissue using our developed combinatorial peptide strategy (Fig. 5a and ESI Data set 4†). In three independent experiments conducted on different mouse brain tissues, the numbers of identified SUMO-1 sites and proteins in the entire brain of the P301S groups all exceeded that in the WT groups (Fig. 5b and c). As shown in Fig. 5d, we categorized SUMO-1 sites into three groups based on the P301S/WT ratio (intensity of SUMO-1 modification sites): P301S Up (ratio ≥ 2.0), P301S Down (ratio ≤ 0.5), and Stable. GO enrichment analysis revealed a significant increase in proteins located in the actin cytoskeleton, centrosome, chromosomal region, and microtubule in the P301S Up group. These proteins exhibited molecular functions such as actin binding, ATP-dependent activity, GTPase regulator activity, and kinase activity (Fig. 5e). Furthermore, the P301S Up group exhibited a notable increase in the number of SUMO-1 modified proteins within specific pathways, particularly autophagy, cholinergic synapse, TNF signaling, and motor proteins. These pathways are closely intertwined with the pathogenesis of AD,[47,48] substantiating the reliability of our methodology. For instance, in the P301S samples, we identified the SUMO-1 modification of two key proteins, Ulk2 (Unc-51-like kinase 2), and Atg2 (Autophagy-related protein 2), within the autophagy pathway.[49] Ulk2, a member of the Unc-51-like kinase family, serves as an initiator kinase in autophagy initiation by forming a complex with other autophagy-related proteins.[50] It phosphorylates and activates the downstream target, Beclin-1, promoting the nucleation of the phagophore, the precursor structure to the autophagosome. Concurrently, Atg2 plays a pivotal role in autophagosome

expansion, retrieving lipids from the endoplasmic reticulum (ER) and other membrane sources to facilitate the elongation of the phagophore membrane.[51] This critical process is essential for the formation of fully functional autophagosomes capable of encapsulating cargoes for degradation, thereby influencing the hyperphosphorylated tau formation and accumulation within cells and exacerbating AD (Fig. 5f).[52]

Additionally, we evaluated the reproducibility of identification and quantification across these biological replicates. The overlap of identified SUMO-1 sites between any two of the three replicates in the AD group ranged from 25% to 30%, and the quantitative correlation of site intensities was between 0.7 and 0.8 (Fig. S17 in the ESI†). Considering the dynamic nature and low abundance of SUMO-1 modifications in vivo, as well as the potential randomness in enrichment and identification, this level of reproducibility is reasonable. When combined with biological validations, our enrichment method can provide valuable insights into the regulatory roles and molecular functions of SUMO-1. Therefore, to further validate our proteomic findings, we conducted co-immunoprecipitation (Co-IP) to detect SUMO-1 modification of Ulk2 in the brains of AD mice. As illustrated in Fig. 6a, AD mouse brain tissue total proteins were divided into two groups: one undergoing conventional Co-IP experiments and the other undergoing **M1** material enrichment before Co-IP, in which **M1** was used to pre-enrich SUMO-1 and its associated substrates. The results of subsequent immunoblot analyses confirmed the presence of SUMO-1 modification in Ulk2 within the brains of AD mice (Fig. 6b). This validation underscores the success and precision of our proteomic strategy. More AD-related SUMO-1 modified proteins and sites are presented in ESI Data set 4.† Overall, our extensive analysis unveils the nuanced involvement of SUMOylation across diverse cellular processes, particularly within the intricate landscape of AD-related pathways.

### SUMO-1 fluorescence imaging

Beyond serving as an enrichment tool, we further explored the versatile applications of the peptide ligands. Based on the aforementioned proteomic findings, we observed that PEP-4 could interact with DV12, the SUMO-1 residual fragment generated by trypsin cleavage. This observation led us to hypothesize that PEP-4 might bind to the entire SUMO-1 protein through its association with this fragment. Consequently, the BLI test was conducted to assess the binding affinity between PEP-4 and the SUMO-1 protein. As depicted in Fig. 6c, PEP-4 indeed displays strong adsorption and weak dissociation to the SUMO-1 protein, with a $K_D$ value of 43.7 nM through a non-linear fitting (Fig. 6d), and their possible binding model is shown in the Fig. 6d inset. This result encouraged the application of PEP-4 in various SUMO-1 related studies, potentially replacing antibody-dependent investigations.

Then, we propose a proof of concept of employing PEP-4 for SUMO-1 imaging. For comparative purposes, we selected a commercially available SUMO-1 antibody (Y299; ab32058, Abcam) as a control, with its binding site over-lapping DV12 (Fig. 6e), facilitating meaningful comparisons. We assessed the
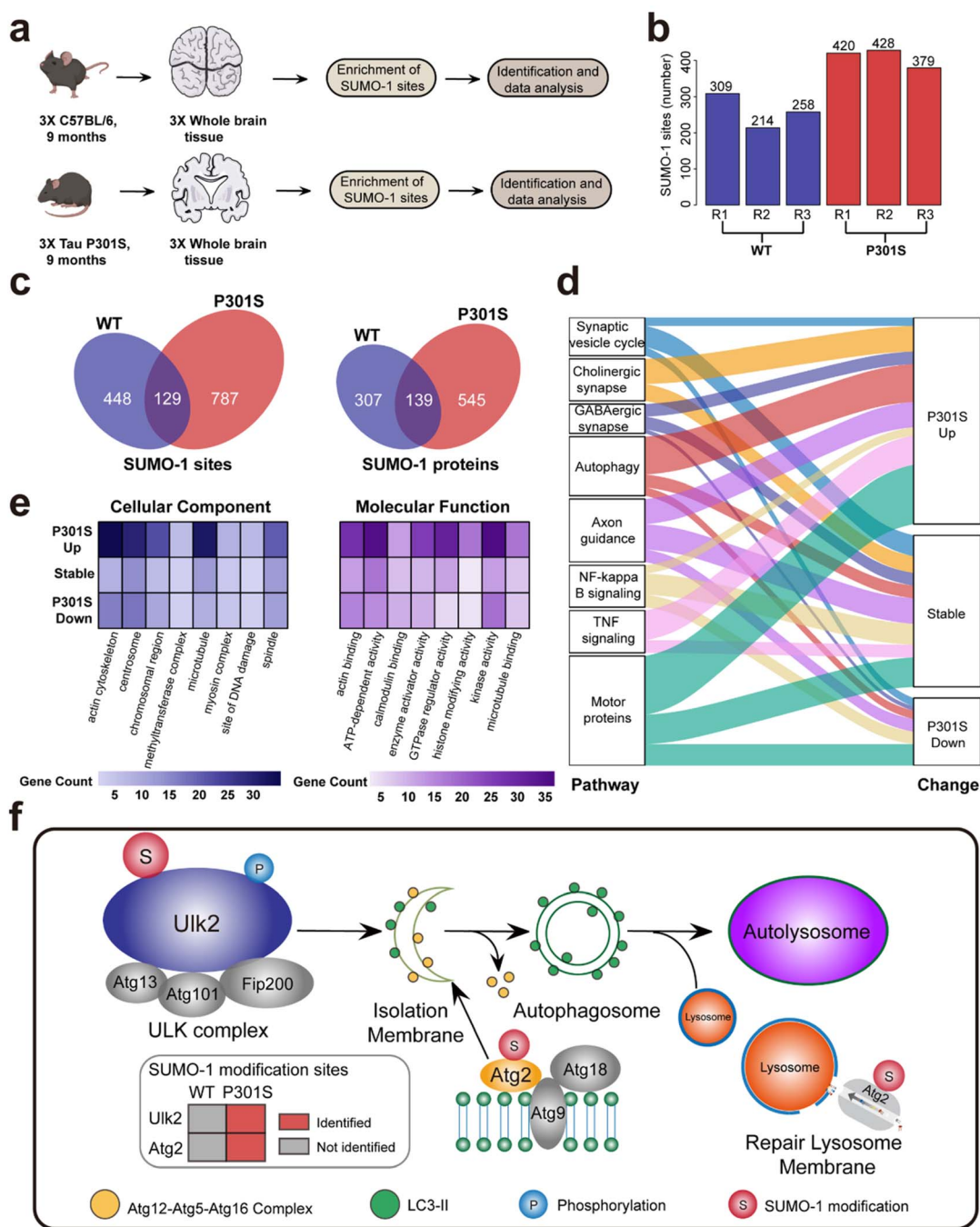
**Fig. 5** Identification of endogenous SUMO-1 sites in mouse brains. (a) Workflows for identifying SUMO-1 sites in mouse brains (WT vs. P301S). (b) Numbers of identified SUMO-1 sites per biological replicate from WT (blue) and P301S (red) groups. (c) Comparison of SUMO-1 modified sites (left) and proteins (right) in WT (blue) and P301S (red) groups. (d) Sankey diagram illustrating the signaling pathways involved in the three group proteins (P301S Up, Stable, P301S Down). (e) GO enrichment analysis (cellular component and molecular function) of SUMO-1 modified proteins. (f) Possible mechanism mediated by SUMO-1 modification for the formation of fully functional autophagosomes capable of encapsulating cargoes for degradation. In the P301S samples, two key proteins, Ulk2 and Atg2 within the autophagy pathway were identified by SUMO-1 modification.

ability of PEP-4 to detect the sub-cellular localization of SUMO-1 through immunofluorescence experiments. As depicted in Fig. 6f, both Y299 and fluorescein amidite labeled PEP-4 (FAM-PEP-4) pre-dominantly localized to the cell nucleus, and FAM-PEP-4 exhibits a nuclear signal clearer than that of the Y299 antibody. Furthermore, FAM-labeled PEP-4 was observed in the

nucleolus, corresponding to SUMO-1 localization. Given that SUMO-1 is primarily distributed in the cell nucleus, with the nucleolus being a site where SUMO-1 modifications mainly occur on ribosomes and chromosomes,[53] these data suggested that PEP-4 could effectively substitute specific antibodies and accurately localize SUMO-1 within cells.
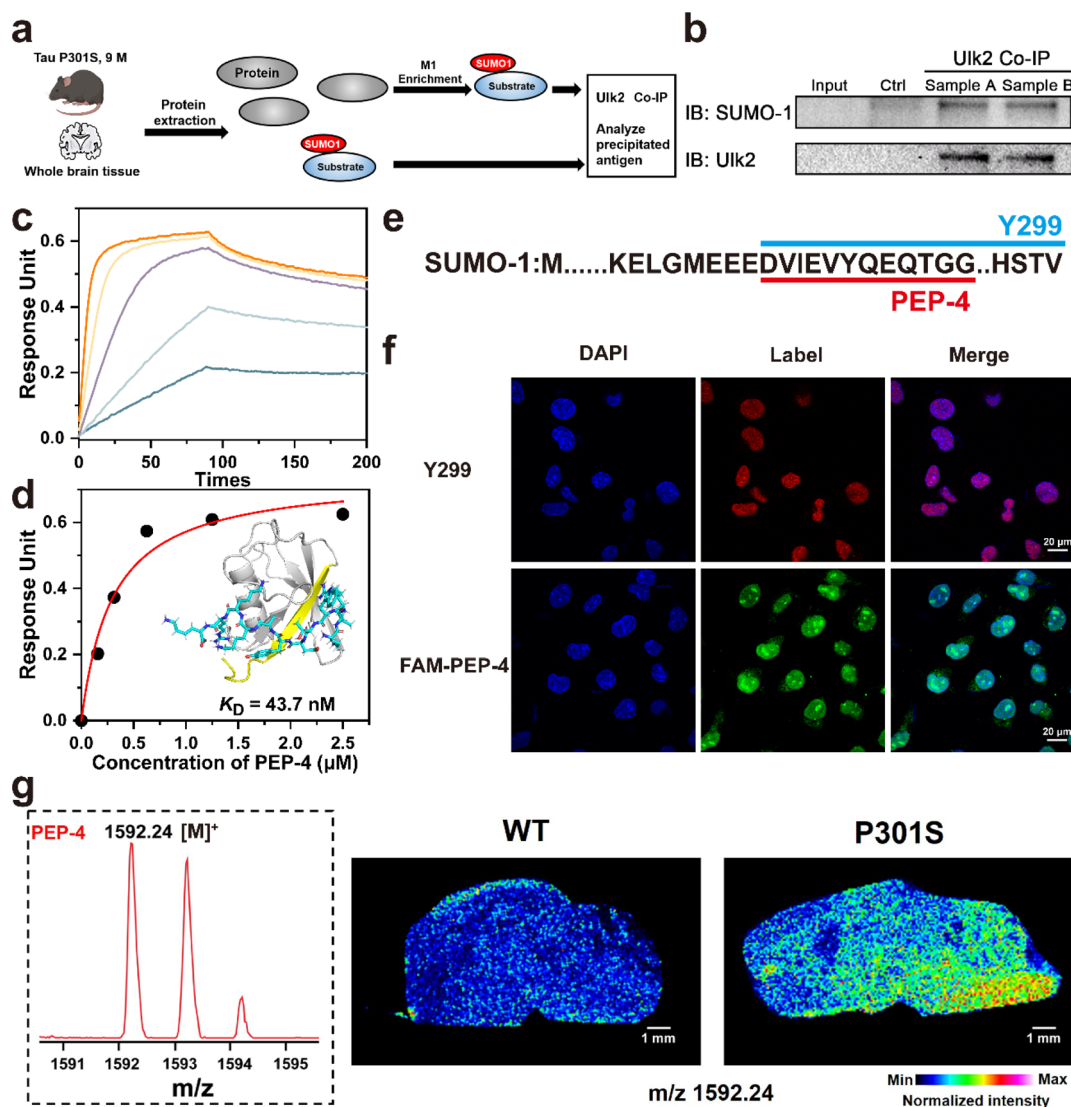
**Fig. 6** Exploring the versatile applications of peptide ligands. (a) Workflow of the Ulk2 Co-IP assay and grouping. (b) Representative Ulk2 Co-IP assay results showing the interaction of Ulk2 with SUMO-1. IB: immunoblotting; Input: total protein lysates from Tau P301S mouse brain tissue; Ctrl: protein lysates incubated without anti-Ulk2 antibody (negative control); Sample A: protein lysates incubated with anti-Ulk2 antibody; Sample B: protein lysates pre-incubated with M1 before the Ulk2 Co-IP experiment. (c) PEP-4 association and dissociation kinetics at different concentrations (0.15, 0.3, 0.625, 1.25, and 2.5 μM) on SUMO-1-modified sensor surfaces, recorded by BLI tests. (d) Fitting curves of BLI tests. PEP-4 showed a strong binding affinity ($K_D$) of 43.7 nM with the SUMO-1 protein. The inset depicts the possible binding model between the SUMO-1 protein (PDB : 2ASQ) and PEP-4, demonstrating the interaction *via* the terminal residues of SUMO-1. (e) Binding site overlap between PEP-4 and SUMO-1 antibody. (f) Imaging of SUMO-1 with PEP-4 in SH-SY5Y cells. 4′, 6-diamidino-2-phenylindole (DAPI) was used to display the localization of the nucleus. SUMO-1 antibody was used as a positive control. FAM-PEP-4 was used for immunofluorescence imaging. Scale bars: 20 μm. (g) MSI visualization for SUMO-1 and SUMO-1 modifications in WT (left) and P301S (right) mouse brain sagittal sections for signals at *m/z* 1592.24. Spectra were normalized against the total ion current (TIC) of all data points.

## Mass spectrometry imaging (MSI)

Based on these results, we extended the application of the peptide to the more challenging MSI, which provides a powerful method for studying the spatial distribution of proteins and their PTMs in biological tissues.[54] However, direct imaging of large protein molecules is impractical, necessitating complex analysis methods for accurate identification.[55,56] In contrast, smaller peptide molecules produce clearer spectra, enhancing identification accuracy. Therefore, leveraging the specific affinity of PEP-4 for SUMO-1 and its modifications, we employed

PEP-4 for the localization of SUMO-1 using MALDI-MSI. As illustrated in Fig. 6g, we successfully charted the comprehensive brain distribution of SUMO-1 and its modified forms in two groups of mice: C57BL/6 wild type (WT) and Tau P301S, representing healthy and AD model mice, respectively, upon labeling with PEP-4. Distinct PEP-4 signals corresponding to SUMO-1 were observed on brain sagittal sections. Importantly, SUMO-1 and its modifications exhibited significant upregulation in the brains of P301S mice compared to WT counterparts, consistent with our proteomic identification results. This further

underscores the involvement of SUMO-1 in AD pathogenesis and its widespread distribution in the brain, highlighting its pivotal regulatory roles in cellular functions and signaling pathways. These results underscore the potential application of our peptide in MSI. Notably, our peptide is equally applicable if specific protein expression in brain regions relevant to certain disease states is of interest, demonstrating the robustness and promising prospects of our peptide.

## Conclusions

Here, to tackle the knotty enrichment challenges of endogenous SUMO-1 modified peptides, we precisely design and propose a novel combinatorial peptide strategy which is applicable to both cellular and tissue contexts. Employing phage display, we successfully identified two novel peptide ligands, PEP-4 and CP-1, specifically designed to target two SUMO-1 remnants at the C-terminal region. These ligands exhibited exceptional affinities for SUMO-1 modified peptide segments. Combining the properties of these ligands, we developed the first artificial SUMO-1 enrichment materials, ultimately establishing a combinatorial peptide strategy that facilitates a comprehensive analysis of endogenous SUMO-1 modified proteomics across species. Unlike existing methods that rely on antibodies with limited specificity and availability, our enrichment strategy leverages peptide ligand-based materials, which display excellent performance in the capture of SUMO-1 peptides.

This study represents the most comprehensive exploration to date of endogenous SUMO-1 modified proteomics, effectively bridging the gap between SUMO-2/3 and other PTM proteomics. Our method provides a robust tool for elucidating the biological significance of SUMO-1 modification, enabling the discovery of new biologically relevant findings and offering substantial potential. The SUMO-1 sites we identified are highly relevant to critical diseases, including cancers and AD. Notably, we discovered a close association between SUMO-1 modification and AD, enabling the first delineation of SUMO-1 distribution in AD mouse brains, which revealed significant upregulation. The success of our proteomic strategy in AD mouse models provides a valuable resource to the field, offering critical insights into the roles of SUMO proteins in diseases and physiology. This, in turn, presents potential therapeutic targets and novel biomarkers for further exploration, ultimately enhancing our understanding of the functional role of SUMOylation in health and disease. This represents a significant advancement in PTM proteomics, offering an invaluable resource for future research. Our group has already applied this strategy to investigate SUMO-1 modifications in the blood of amyotrophic lateral sclerosis (ALS) patients, uncovering promising insights that could further illuminate the role of SUMOylation in neurode-generative diseases.

Moreover, by successfully identifying specific peptide ligands for SUMO-1 modified peptide segments, we unlock new possibilities for their application in identifying modified peptides (e.g., QPTGG in SUMO4, QIGG in SUMO5) and other challenging PTMs, setting a precedent for their future applications in PTM proteomics. For diverse targets, such as shorter amino acid sequences or smaller molecules, selecting the appropriate peptide library and optimizing screening strategies and conditions can enable the identification of specific ligands for various motifs, thereby enhancing the versatility of phage display technology.

Looking forward, the identified peptides hold promise for development in various applications, including SUMO-1 targeting drug release systems, SUMO-1 probes, bioimaging, and drug design. Moreover, the versatility demonstrated by our peptides suggests that similar peptide ligand approaches could find valuable applications in various PTM studies with unique regulatory effects similar to that of SUMOylation, yet remain challenging to efficiently capture.[57–59] For example, coupling specific peptide ligand recognition units with magnetic nano-particles could enhance the enrichment analysis of low-abundance peptides or proteins.[60–62] Similarly, integration with microfluidics or nanopore sensors could enable single-cell multi-omics studies,[63,64] highlighting promising avenues for future exploration.

## Data availability

The data supporting the findings of this study are available within the article and in the ESI.† Mass spectrometry RAW data are available at the ProteomeXchange Consortium database via the iProX partner repository with the dataset identifier PXD050705.

## Author contributions

Y. Z. provided academic guidance and the research direction. X. Z., B. J., L. Z., and G. Q. conceived and directed the project. G. Q. developed the concept and designed experiments. X. Z. and B. Z. performed most of the experiments. Y. S. assisted in the preparation of enrichment materials and co-immunoprecipitation experiments. D. L. performed mass spectrometry imaging experiments. X. Z. helped to perform phage display biopanning. D. W. performed molecular dynamics simulations. C. W. assisted with the immunofluorescence experiments. H. G. and M. Z. provided mice tissues. H. Q., Z. Y., and X. Y. performed NMR experiments. Y. C. helped to perform ITC experiments. Y. L. and H. W. improved part of the figures of the manuscript. X. Z. wrote the manuscript. B. Z., B. J., and G. Q revised the manuscript. All the authors provided critical comments on the manuscript.

## Conflicts of interest

There are no conflicts to declare.

## Acknowledgements

## Notes and references

1 C. Li, F. P. McManus, C. Plutoni, C. M. Pascariu, T. Nelson, L. E. Alberici Delsin, G. Emery and P. Thibault, *Nat. Commun.*, 2020, **11**, 834.

2 Y. Z. Wang, X. Liu, G. Way, V. Madarha, Q. T. Zhou, D. H. Yang, J. Y. Liao and M. W. Wang, *Acta Pharmacol. Sin.*, 2020, **41**, 1497–1506.

3 A. B. Celen and U. Sahin, *FEBS J.*, 2020, **287**, 3110–3140.

4 R. Geiss-Friedlander and F. Melchior, *Nat. Rev. Mol. Cell Biol.*, 2007, **8**, 947–956.

5 I. A. Hendriks and A. C. Vertegaal, *Nat. Rev. Mol. Cell Biol.*, 2016, **17**, 581–595.

6 A. C. O. Vertegaal, *Nat. Rev. Mol. Cell Biol.*, 2022, **23**, 715–731.

7 H. Saitoh and J. Hinchey, *J. Biol. Chem.*, 2000, **275**, 6252–6258.

8 L. Cai, J. Tu, L. Song, Z. Gao, K. Li, Y. Wang, Y. Liu, F. Zhong, R. Ge, J. Qin, et al., *Mol. Cell. Proteomics*, 2017, **16**, 717–727.

9 J. Becker, S. V. Barysch, S. Karaca, C. Dittner, H. H. Hsiao, M. Berriel Diaz, S. Herzig, H. Urlaub and F. Melchior, *Nat. Struct. Mol. Biol.*, 2013, **20**, 525–531.

10 B. Bodenmiller, L. N. Mueller, M. Mueller, B. Domon and R. Aebersold, *Nat. Methods*, 2007, **4**, 231–237.

11 Y. Oda, T. Nagasu and B. T. Chait, *Nat. Biotechnol.*, 2001, **19**, 379–382.

12 L. Hwang, S. Ayaz-Guner, Z. R. Gregorich, W. Cai, S. G. Valeja, S. Jin and Y. Ge, *J. Am. Chem. Soc.*, 2015, **137**, 2432–2435.

13 W. Kim, E. J. Bennett, E. L. Huttlin, A. Guo, J. Li, A. Possemato, M. E. Sowa, R. Rad, J. Rush, M. J. Comb, et al., *Mol. Cell*, 2011, **44**, 325–340.

14 L. K. Povlsen, P. Beli, S. A. Wagner, S. L. Poulsen, K. B. Sylvestersen, J. W. Poulsen, M. L. Nielsen, S. Bekker-Jensen, N. Mailand and C. Choudhary, *Nat. Cell Biol.*, 2012, **14**, 1089–1098.

15 D. F. Zielinska, F. Gnad, J. R. Wiśniewski and M. Mann, *Cell*, 2010, **141**, 897–907.

16 Y. Watanabe, J. D. Allen, D. Wrapp, J. S. McLellan and M. Crispin, *Science*, 2020, **369**, 330–333.

17 L. R. Ruhaak, G. Xu, Q. Li, E. Goonatilleke and C. B. Lebril-la, *Chem. Rev.*, 2018, **118**, 7886–7930.

18 C. Choudhary, C. Kumar, F. Gnad, M. L. Nielsen, M. Rehman, T. C. Walther, J. V. Olsen and M. Mann, *Science*, 2009, **325**, 834–840.

19 E. S. Witze, W. M. Old, K. A. Resing and N. G. Ahn, *Nat. Methods*, 2007, **4**, 798–806.

20 J. Brandi, R. Noberini, T. Bonaldi and D. Cecconi, *J. Chromatogr. A*, 2022, **1678**, 463352.

21 H. A. Blomster, S. Y. Imanishi, J. Siimes, J. Kastu, N. A. Morrice, J. E. Eriksson and L. Sistonen, *J. Biol. Chem.*, 2010, **285**, 19324–19329.

22 R. Bruderer, M. H. Tatham, A. Plechanovova, I. Matic, A. K. Garg and R. T. Hay, *EMBO Rep.*, 2011, **12**, 142–148.

23 F. Lamoliatte, D. Caron, C. Durette, L. Mahrouche, M. A. Maroui, O. Caron-Lizotte, E. Bonneil, M. K. Chelbi-Alix and P. Thibault, *Nat. Commun.*, 2014, **5**, 5409.

24 R. J. Lumpkin, H. Gu, Y. Zhu, M. Leonard, A. S. Ahmad, K. R. Clauser, J. G. Meyer, E. J. Bennett and E. A. Komives, *Nat. Commun.*, 2017, **8**, 1171.

25 I. A. Hendriks, D. Lyon, D. Su, N. H. Skotte, J. A. Daniel, L. J. Jensen and M. L. Nielsen, *Nat. Commun.*, 2018, **9**, 2456.

26 C. Díaz-Perlas, B. Ricken, L. Farrera-Soler, D. Guschin, F. Pojer, K. Lau, C. B. Gerhold and C. Heinis, *Nat. Commun.*, 2023, **14**, 2774.

27 B. Liu, S. Jiang, M. Li, X. Xiong, M. Zhu, D. Li, L. Zhao, L. Qian, L. Zhai, J. Li, et al., *Nat. Commun.*, 2018, **9**, 4770.

28 G. P. Smith, *Angew. Chem., Int. Ed.*, 2019, **58**, 14428–14437.

29 S. S. Kale, C. Villequey, X. D. Kong, A. Zorzi, K. Deyle and C. Heinis, *Nat. Chem.*, 2018, **10**, 715–723.

30 Y. Zhang, M. Fang, S. Li, H. Xu, J. Ren, L. Tu, B. Zuo, W. Yao and G. Liang, *Mol. Cancer*, 2022, **21**, 158.

31 A. S. Pina, L. Morgado, K. L. Duncan, S. Carvalho, H. F. Carvalho, A. J. M. Barbosa, P. M. B. de, I. P. Moreira, D. Kalafatovic, B. M. Morais Faustino, et al., *Chem. Sci.*, 2021, **13**, 210–217.

32 T. Li, H. Cai, H. Yao, B. Zhou, N. Zhang, M. F. van Vlissingen, T. Kuiken, W. Han, C. H. GeurtsvanKessel, Y. Gong, et al., *Nat. Commun.*, 2021, **12**, 4635.

33 N. Li, H. Fu, S. M. Hewitt, D. S. Dimitrov and M. Ho, *Proc. Natl. Acad. Sci. U.S.A.*, 2017, **114**, E6623–e6631.

34 Y. Li, M. Sun, Y. Hu, Y. Shan, Z. Liang, L. Zhang and Y. Zhang, *Anal. Chim. Acta*, 2021, **1154**, 338324.

35 Z. Shi, X. Zhang, X. Yang, X. Zhang, F. Ma, H. Gan, J. Chen, D. Wang, W. Sun, J. Wang, et al., *Adv. Mater.*, 2023, **35**, e2302560.

36 W. Qin, W. Zhang, L. Song, Y. Zhang and X. Qian, *Anal. Chem.*, 2010, **82**, 9461–9468.

37 Y. Zhou, B. Zhou, L. Pache, M. Chang, A. H. Khodabakhshi, O. Tanaseichuk, C. Benner and S. K. Chanda, *Nat. Commun.*, 2019, **10**, 1523.

38 M. S. Rodriguez, C. Dargemont and R. T. Hay, *J. Biol. Chem.*, 2001, **276**, 12654–12659.

39 F. Impens, L. Radoshevich, P. Cossart and D. Ribet, *Proc. Natl. Acad. Sci. U.S.A.*, 2014, **111**, 12432–12437.

40 Z. Xue, D. J. Vis, A. Bruna, T. Sustic, S. van Wageningen, A. S. Batra, O. M. Rueda, E. Bosdriesz, C. Caldas, L. F. A. Wessels, et al., *Cell Res.*, 2018, **28**, 719–729.

41 R. A. Jansen, S. Mainardi, M. H. Dias, A. Bosma, E. van Dijk, R. Selig, W. Albrecht, S. A. Laufer, L. Zender and R. Bernards, *Proc. Natl. Acad. Sci. U.S.A.*, 2024, **121**, e2319492121.

42 H. Han, J. W. Cho, S. Lee, A. Yun, H. Kim, D. Bae, S. Yang, C. Y. Kim, M. Lee, E. Kim, et al., *Nucleic Acids Res.*, 2018, **46**, D380–d386.

43 S. A. Kent, T. L. Spires-Jones and C. S. Durrant, *Acta Neuropathol.*, 2020, **140**, 417–447.

44 C. W. Chang, E. Shao and L. Mucke, *Science*, 2021, **371**, 6532.

45 K. Takahashi, M. Ishida, H. Komano and H. Takahashi, *Neurosci. Lett.*, 2008, **441**, 90–93.

46 H. B. Luo, Y. Y. Xia, X. J. Shu, Z. C. Liu, Y. Feng, X. H. Liu, G. Yu, G. Yin, Y. S. Xiong, K. Zeng, *et al.*, *Proc. Natl. Acad. Sci. U.S.A.*, 2014, **111**, 16586–16591.

47 J. M. Long and D. M. Holtzman, *Cell*, 2019, **179**, 312–339.

48 S. L. Morgan, P. Naderi, K. Koler, Y. Pita-Juarez, D. Prokopenko, I. S. Vlachos, R. E. Tanzi, L. Bertram and W. A. Hide, *Front. Aging Neurosci.*, 2022, **14**, 846902.

49 Z. Zhang, X. Yang, Y. Q. Song and J. Tu, *Ageing Res. Rev.*, 2021, **72**, 101464.

50 Y. Lu, J. Xu, Y. Li, R. Wang, C. Dai, B. Zhang, X. Zhang, L. Xu, Y. Tao, M. Han, *et al.*, *Sci. Transl. Med.*, 2024, **16**, eade8647.

51 J. Sawa-Makarska, V. Baumann, N. Coudevylle, S. von Bülow, V. Nogellova, C. Abert, M. Schuschnig, M. Graef, G. Hummer and S. Martens, *Science*, 2020, **369**, 6508.

52 A. S. Gross, R. Ghillebert, M. Schuetter, E. Reinartz, A. Rowland, B. C. Bishop, M. Stumpe, J. Dengjel and M. Graef, *Nat. Cell Biol.*, 2024, **26**, 366–377.

53 M. P. C. Mulder, R. Merkx, K. F. Witting, D. S. Hameed, D. El Atmioui, L. Lelieveld, F. Liebelt, J. Neefjes, I. Berlin, A. C. O. Vertegaal, *et al.*, *Angew. Chem., Int. Ed.*, 2018, **57**, 8958–8962.

54 K. Schwamborn and R. M. Caprioli, *Mol. Oncol.*, 2010, **4**, 529–538.

55 Y. R. Xie, D. C. Castro, S. S. Rubakhin, T. J. Trinklein, J. V. Sweedler and F. Lam, *Nat. Methods*, 2024, **21**, 521–530.

56 E. M. Unterauer, S. Shetab Boushehri, K. Jevdokimenko, L. A. Masullo, M. Ganji, S. Sograte-Idrissi, R. Kowalewski, S. Strauss, S. C. M. Reinhardt, A. Perovic, *et al.*, *Cell*, 2024, **187**, 1785–1800.

57 T. Wang, S. Ma, G. Ji, G. Wang, Y. Liu, L. Zhang, Y. Zhang and H. Lu, *Nat. Commun.*, 2024, **15**, 2997.

58 M. Li, Y. Xiong and G. Qing, *Acc. Chem. Res.*, 2023, **56**, 2514–2525.

59 Y. Li, Y. Sun, X. Zhang, D. Wang, X. Yang, H. Wei, C. Wang, Z. Shi, X. Li, F. Zhang, W. Sun, Z. Yang, Y. Song and G. Qing, *ACS Appl. Mater. Interfaces*, 2024, **16**, 47110–47123.

60 T. N. Tiambeng, D. S. Roberts, K. A. Brown, Y. Zhu, B. Chen, Z. Wu, S. D. Mitchell, T. M. Guardado-Alvarez, S. Jin and Y. Ge, *Nat. Commun.*, 2020, **11**, 3903.

61 J. Xu, G. Feng, D. Ao, X. Li, M. Li, S. Lei and Y. Wang, *Adv. Mater.*, 2024, **36**, 2406256.

62 M. Li, Y. Xiong and G. Qing, *Trends Anal. Chem.*, 2020, **124**, 115585.

63 W. Liu, Z. Yang, C. Yang, Y. Ying and Y. Long, *Chem. Sci.*, 2022, **13**, 4109–4114.

64 T. Xie, Q. Zhang, W. Zhang, S. Feng and J. M. Lin, *Small*, 2020, **18**, e2107992.